

SURVIVAL OF AMORPHOUS WATER ICE ON CENTAURS

AURÉLIE GUILBERT-LEPOUTRE

Department of Earth and Space Sciences, UCLA, Los Angeles, CA 90095, USA; aguilbert@ucla.edu

Received 2012 March 12; accepted 2012 July 24; published 2012 August 30

ABSTRACT

Centaur objects are believed to be Kuiper Belt objects in transition between Jupiter and Neptune before possibly becoming Jupiter family comets. Some indirect observational evidence is consistent with the presence of amorphous water ice in Centaurs. Some of them also display a cometary activity, probably triggered by the crystallization of the amorphous water ice, as suggested by Jewitt and this work. Indeed, we investigate the survival of amorphous water ice against crystallization, using a fully three-dimensional thermal evolution model. Simulations are performed for varying heliocentric distances and obliquities. They suggest that crystallization can be triggered as far as 16 AU, though amorphous ice can survive beyond 10 AU. The phase transition is an efficient source of outgassing up to 10–12 AU, which is broadly consistent with the observations of the active Centaurs. The most extreme case is 167P/CINEOS, which barely crystallizes in our simulations. However, amorphous ice can be preserved inside Centaurs in many heliocentric distance–obliquity combinations, below a ~ 5 –10 m crystallized crust. We also find that outgassing due to crystallization cannot be sustained for a time longer than 10^4 – 10^5 years, leading to the hypothesis that active Centaurs might have recently suffered from orbital changes. This could be supported by both observations (although limited) and dynamical studies.

Key words: comets: general – Kuiper Belt: general – methods: numerical

Online-only material: color figures

1. INTRODUCTION

Centaur objects are a population of small bodies in the outer solar system, orbiting in the giant planets region. In this work, we define Centaurs as objects orbiting between Jupiter and Neptune, with the following constraints on their perihelion distance q and semimajor axis a : $q_J < q < q_N$ and $a_J < a < a_N$. They experience repeated close encounters with giant planets, resulting in short-lived chaotic orbits. Centaur orbits are typically stable on timescales ranging from a few million years to a hundred million years (Levison & Duncan 1997; Tiscareno & Malhotra 2003; Horner et al. 2004; di Sisto & Brunini 2007). They are therefore a transient population of recent escapees from a source region possibly further out in the solar system, like the Kuiper Belt or the Scattered Disk (Levison & Duncan 1997; Volk & Malhotra 2008), or possibly from the Trojan clouds (Horner & Lykawka 2010). The fate of Centaurs could be to impact a giant planet or being broken apart by gravitational stresses. More than two-thirds can escape the solar system (Tiscareno & Malhotra 2003), and the rest could become Jupiter family comets (JFCs). Centaurs offer the possibility to study some of the most primordial material in the solar system. They are more accessible than Kuiper Belt objects, and more stable from a physical point of view than JFCs, whose lifetime is limited by different dynamical and physical processes.

Some observational evidence, albeit indirect, are consistent with the presence of amorphous water ice in both comets (Meech et al. 2009) and Centaurs (Jewitt 2009). Some Centaurs display comet-like activity, even though they are orbiting beyond the snowline, the limit beyond which water ice is thermodynamically stable. Their mass loss is therefore not driven by water-ice sublimation. A recent study on active Centaurs showed that their activity could be thermally driven, meaning that the trigger for mass loss is a temperature-related process (Jewitt 2009). The results suggest that crystallization of amorphous water ice is a plausible explanation for the activity of Centaurs. It is there-

fore interesting to understand whether amorphous water ice can survive on Centaurs. Amorphous water ice can persist for timescales comparable to the age of the solar system because the rate of phase transition $\lambda(T)$ depends on the temperature, determined by an activation law found experimentally by Schmitt et al. (1989):

$$\lambda(T) = 1.05 \times 10^{13} e^{-5370/T} \text{ s}^{-1}. \quad (1)$$

Amorphous water ice also has the ability to trap large amounts of volatiles that can be expelled upon crystallization (Bar-Nun et al. 1985; Laufer et al. 1987; Hudson & Donn 1991; Jenniskens & Blake 1994; Notesco & Bar-Nun 1996; Bar-Nun & Owen 1998; Notesco et al. 2003). The phase transition is an exothermic and irreversible process, which could be the source of activity in the giant planet regions, where the equilibrium temperature is too low for water ice to sublimate.

In this paper, we use a fully three-dimensional model of small bodies thermal evolution to study the occurrence of crystallization at the surface and in the interior of Centaurs. We follow the idea developed by Jewitt (2009) that crystallization is the driver for Centaur activity, and investigate the effect of orbital parameters on the process to understand how amorphous water ice can survive in this region of the solar system. Section 2 briefly presents the model, Sections 3 and 4 give results from the modeling compared to observations concerning the presence of crystalline and amorphous water at the surface of Centaurs and crystallization as a source of cometary activity among them.

2. THERMAL EVOLUTION MODEL

We use a model of Centaurs in which the parameters are idealized in order to make the problem tractable. We consider that the objects—50 km bodies with a 10 hr rotation period—are initially spheres made of a porous mixture of water ice and dust grains. We assume the ice to be initially amorphous, which also assumes a cold accretion and no previous thermal alteration due

Table 1
Heat Capacities and Thermal Conductivities

| Parameters | Value | Unit | References |
|--------------------------|--|----------------------------------|------------|
| $c_{\text{H}_2\text{O}}$ | $7.49 T + 90$ | $\text{J kg}^{-1} \text{K}^{-1}$ | G&S36 |
| c_d | 1200 | $\text{J kg}^{-1} \text{K}^{-1}$ | E&S83 |
| κ_a | $2.34 \times 10^{-3} T + 2.8 \times 10^{-2}$ | $\text{W m}^{-1} \text{K}^{-1}$ | K180 |
| κ_{cr} | $567/T$ | $\text{W m}^{-1} \text{K}^{-1}$ | K180 |
| κ_d | 4.2 | $\text{W m}^{-1} \text{K}^{-1}$ | E&S83 |
| c_{init} | 830 | $\text{J kg}^{-1} \text{K}^{-1}$ | |
| κ_{init} | 6.4×10^{-2} | $\text{W m}^{-1} \text{K}^{-1}$ | |

Notes. T : temperature [K]. $c_{\text{H}_2\text{O}}$, c_d : heat capacity for water ice and for dust, respectively. κ_a , κ_{cr} , κ_d : thermal conductivities of amorphous and crystalline water ice, and dust, respectively. c_{init} and κ_{init} : initial values of the heat capacity and thermal conductivity.

References. G&S36: Giauque & Stout (1936); E&S83: Ellsworth & Schubert (1983); K180: Klinger (1980).

to radioactive decay. The bulk material can be described with a dust to water ice mass ratio $X_d/X_{\text{H}_2\text{O}} = 1$, a porosity $\psi = 30\%$, and a bulk density $\rho_{\text{bulk}} = 1 \text{ g cm}^{-3}$. The heat capacity of the mixture is obtained by averaging the values weighted by the mass fraction of each component:

$$c = X_{\text{H}_2\text{O}}c_{\text{H}_2\text{O}} + X_dc_d, \quad (2)$$

with $X_{\text{H}_2\text{O}}$ and X_d the mass fraction of water ice and dust, and $c_{\text{H}_2\text{O}}$ and c_d [$\text{J kg}^{-1} \text{K}^{-1}$] the heat capacities of each component. The numerical values used in this work can be found in Table 1. The thermal conductivity is obtained by considering the material as made of two phases, the empty pores with a thermal conductivity $\kappa_p = 4r_p\varepsilon\sigma T^3$ (Huebner et al. 2006), with $r_p = 1 \mu\text{m}$ the average pore radius, $\varepsilon = 0.9$ the medium emissivity, σ the Stefan–Boltzmann constant and T [K] the temperature, and the solid matrix with a thermal conductivity κ_s . The latter is computed as follows:

$$\kappa_s = x_{\text{H}_2\text{O}}[(1 - X_{\text{cr}})\kappa_a + X_{\text{cr}}\kappa_{\text{cr}}] + x_d\kappa_d, \quad (3)$$

with $x_{\text{H}_2\text{O}}$ and x_d the volume fractions of water ice and dust, respectively, and X_{cr} the mass fraction of crystalline water ice. The material effective thermal conductivity accounts for the effects of the solid granularity (through the Hertz factor) and porosity (see Guilbert-Lepoutre et al. 2011 for details).

The model is fully described in Guilbert-Lepoutre et al. (2011). It computes the temperature distribution at the surface and inside the bodies by taking into account three-dimensional heat fluxes. It includes several thermal processes occurring at the surface of the objects, like insolation, described by $(1 - A)S_{\odot}/d_H^2 \cos \xi$, with A the Bond albedo, S_{\odot} the solar constant, d_H the object’s heliocentric distance, $\xi \leq 90^\circ$ the local zenith angle, and thermal emission $\varepsilon\sigma T^4$, with ε material emissivity, σ the Stefan–Boltzmann constant, and T the surface temperature. The model also includes the phase transition between amorphous and crystalline water ice, described by

$$\mathcal{Q}_{\text{cryst}} = \lambda(T)\rho_a H_{\text{ac}} [\text{W m}^{-3}], \quad (4)$$

with ρ_a [kg m^{-3}] the amorphous water ice bulk density. The phase transition releases a latent heat $H_{\text{ac}} = 9 \times 10^4 \text{ J kg}^{-1}$ (Klinger 1981), with a rate given by Equation (1). No sublimation is accounted for, as the objects are too far from the Sun for water ice to sublimate. We therefore solve the following heat

conduction equation:

$$\rho_{\text{bulk}}c \frac{\partial T}{\partial t} + \nabla(-\kappa \nabla T) = \mathcal{Q}_{\text{cryst}}, \quad (5)$$

where T [K] is the temperature distribution to be determined, ρ_{bulk} [kg m^{-3}] is the object’s bulk density, c [$\text{J kg}^{-1} \text{K}^{-1}$] is the material heat capacity, κ [$\text{W m}^{-1} \text{K}^{-1}$] is its effective thermal conductivity, and $\mathcal{Q}_{\text{cryst}}$ [W m^{-3}] is the internal power production per unit volume due to the amorphous-crystalline phase transition.

We investigate the effects of heliocentric distance and obliquity Θ ($\Theta = 0^\circ$ corresponds to the case where the spin axis is normal to the orbital plane, other angles correspond to a tilt of the spin axis toward the Sun at perihelion), on the temperature distribution at the surface and inside of Centaurs. We consider a Bond albedo of 6% (Stansberry et al. 2008), and an initial temperature of 50 K, which is about the equilibrium temperature in the Kuiper Belt. The time 0 in our simulations corresponds to the moment when the objects are placed in the Centaur orbits. We compute the evolution of temperatures for 10 Myr, the average time a Centaur can spend on its orbit before either leaving the solar system or becoming a JFC, due to gravitational interactions with giant planets (Tiscareno & Malhotra 2003; Horner et al. 2004). Our main orbital assumption is that we consider circular orbits. This is justified by the fact that the thermal evolution under insolation is linked to the amount of energy received per orbit (see also Section 4.2). For each eccentric orbit, it is thus possible to compute an equivalent circular orbit with a radius $a_c = a(1 - e^2)$, which receives the same amount of energy per orbit (Prialnik & Rosenberg 2009). Considering circular orbits will therefore allow us to decrease the number of free parameters to investigate, and dress a framework in which any real Centaur, with an eccentric orbit, can be placed through a_c .

3. CRYSTALLIZATION AT THE SURFACE

3.1. Results from Thermal Evolution Simulations

As crystallization of amorphous ice is a temperature-dependent process, it proceeds at different rates depending on the latitude at the surface of Centaurs. For example, for an object with an obliquity $\Theta = 0^\circ$, poles are much colder than the equator and thus the crystallization of ice will be faster in the equatorial regions than the polar regions. Figure 1 gives the distribution of amorphous and crystalline water ice at the surface of Centaurs, as a function of the heliocentric distance (the orbit is circular) and obliquity, after the objects reach a thermal equilibrium (within a few orbits), and the phase transition is being quenched. Amorphous ice can be preserved in the cold polar regions of bodies with $\Theta = 0^\circ$, even if they are close to the Sun (6 AU for instance). When a mixture of amorphous and crystalline water ice is present at the surface, this means that the crystallization process has been triggered but not completed within the time of the simulation. As the heliocentric distance increases, the amount of crystalline water ice in this mixture decreases, due to a slower rate of phase transition. Beyond 14 AU, the surface temperature of an object with $\Theta = 0^\circ$ is too low at any latitude for crystallization to be triggered at the surface within 10 Myr.

An obliquity different from 0° allows variations of the subsolar point latitude across the orbit. With increasing obliquities, higher latitudes on the surface of Centaurs can reach temperatures hot enough to trigger crystallization. This also averages out the temperature at the surface for moderate obliquities

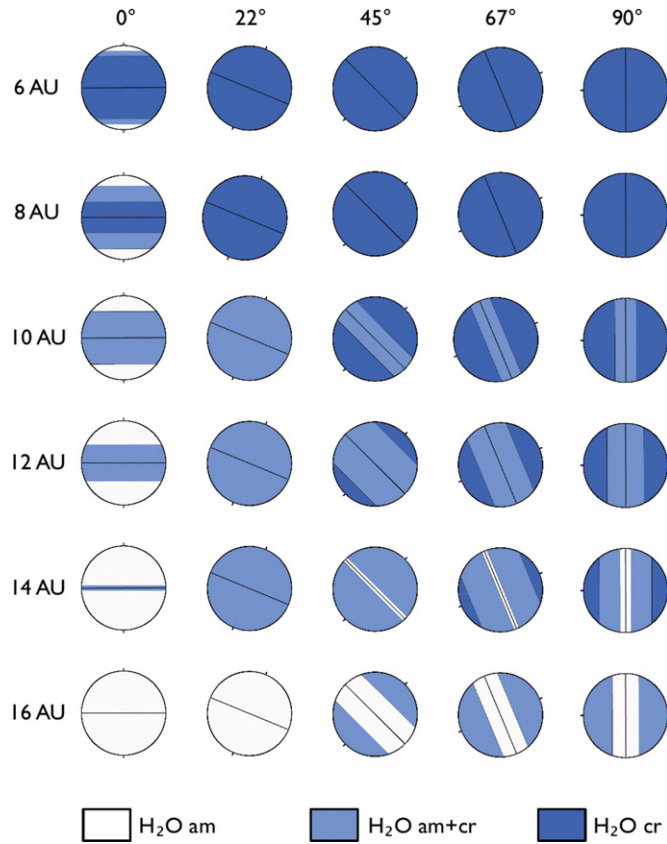


Figure 1. Distributions of amorphous and crystalline water ice at the surface of Centaurs with different heliocentric distances and obliquities, after 10 million years of evolution in the giant planets region. Rows show the different heliocentric distances, columns display the different obliquities.

(A color version of this figure is available in the online journal.)

($\Theta < 45^\circ$). At small heliocentric distances like 6 or 8 AU, the overall surface is crystallized. However, for high obliquities ($\Theta > 45^\circ$), peak temperatures at the equator become lower than peak temperatures in the polar regions. Again, this is a case where the rate of phase transition strongly depends on the latitude, except that the equatorial regions of the surface are able to retain amorphous ice. This effect is clearly seen beyond 10 AU, where crystallization is not completed in the equatorial regions within 10 Myr, and particularly beyond 14 AU where low latitudes around the equator remain completely amorphous. These results also depend on the albedo we considered at the surface of the objects. A higher albedo would prevent crystallization in more configurations, as a lower albedo could lead to crystallization at larger heliocentric distances. The trends for a given albedo, however, would remain the same.

3.2. Surface Composition of Centaurs

The simulations we performed suggest that crystallization of amorphous water ice can be triggered at heliocentric distances as large as 16 AU, for high spin obliquities. However, at these distances, the amount of crystalline water ice at the surface of Centaurs should remain low, meaning that it would not necessarily be detected even by high-quality spectroscopic observations. Large amounts of crystalline water ice could be detected on Centaurs orbiting close to the Sun, or as far as 12 AU if we consider the possibility of high obliquities. The surface composition of Centaurs can be studied through near-infrared spectroscopic observations. Water ice, if present at the surface

Table 2

Water Ice at the Surface of Centaurs, Unveiled by Near-infrared Spectroscopy

| | | Water Ice? | References |
|--------|-----------------------|---|-----------------------------------|
| 2060 | Chiron | Yes ^a (2.0 μm) | Luu94, Fos99, Luu00, Rom03 |
| 5145 | Pholus | Yes (1.5 & 2.0 μm) | Dav93, Luu94, Cru98, Bar08, Bar11 |
| 8405 | Asbolus | No or inconclusive | Bar99 |
| 10199 | Chariklo | Yes ^a (1.5 & 2.0 μm) | Bro98, BrK98, Dot03b, Gui09b |
| 31824 | Elatus | Yes ^a (1.5 & 2.0 μm) | Bau02, Bar08 |
| 32532 | Thereus | Yes ^a (1.5 & 2.0 μm) | Bar02, Lic05, Mer05, Gui09a |
| 52872 | Okyrhoe | No or inconclusive | Dot03a, Bar03, DeM10 |
| 54598 | Bienor | Yes (1.5 & 2.0 μm) | Dot03a, Bar08, Gui09a |
| 55576 | Amycus | No or inconclusive | Dor05, Bar11 |
| 60558 | Echeclus | No or inconclusive | Gui09a |
| 63252 | 2001 BL ₄₁ | No or inconclusive | Dor03 |
| 83982 | Crantor | Yes (2.0 μm) | Dor05, Bar08, Gui09a |
| 95626 | 2002 GZ ₃₂ | No or inconclusive | Bar08, Bar11 |
| 120061 | 2003 CO ₁ | No or inconclusive | Bar11 |
| 250112 | 2002 KY ₁₄ | No or inconclusive | Bar11 |

Notes. ^a Spectral variations reported.

References. Bar08: Barkume et al. (2008); Bar99: Barucci et al. (1999); Bar02: Barucci et al. (2002); Bar11: Barucci et al. (2011); Bau02: Bauer et al. (2002); Bro98: Brown et al. (1998); BrK98: Brown & Koresko (1998); Cru98: Cruikshank et al. (1998); Dav93: Davies et al. (1993); DeM10: DeMeo et al. (2010); Dor03: Doressoundiram et al. (2003); Dor05: Doressoundiram et al. (2005); Dot03b: Dotto et al. (2003b); Dot03a: Dotto et al. (2003a); Fos99: Foster et al. (1999); Gui09a: Guilbert et al. (2009a); Gui09b: Guilbert et al. (2009b); Lic05: Licandro & Pinilla-Alonso (2005); Luu94: Luu et al. (1994); Luu00: Luu et al. (2000); Mer05: Merlin et al. (2005); Rom03: Romon-Martin et al. (2003).

of these objects, would produce detectable absorption bands located at 1.5 and 2.0 μm . An additional band at 1.65 μm is used to track the presence of crystalline water ice. As of today, spectroscopic data are available for only 15 Centaurs, shown in Table 2. For eight of these objects, no water ice can be detected, or the quality of the spectra does not actually allow us to make any conclusive detection. Among the seven other objects whose spectra show water ice features, no 1.65 μm band has ever been reported. However, the quality of the available spectra does not necessarily allow us to detect this feature.

The absence of the 1.65 μm absorption band cannot be used as evidence of the presence of amorphous ice, rather than crystalline water ice. In addition, the presence of the 1.65 μm feature is conditioned by the temperature and irradiation state of the surface, as suggested by Mastrapa & Brown (2006 and reference therein). At low temperatures (<50 K), irradiated crystalline water ice can produce an amorphous water ice spectrum. But for temperatures between 70 and 100 K, irradiated crystalline water ice produces a spectrum almost indistinguishable from the spectrum of crystalline water ice. However, at these temperatures and beyond, the 1.65 μm feature is less strong and sharp than at low temperatures. By combining these results, it remains hard to understand if the 1.65 μm feature can actually be detected in Centaurs' spectra, due to their intermediate surface temperatures and the intermediate irradiation doses they receive (see Hudson et al. 2008). However, it is reasonable to deem that the presence of a 1.65 μm absorption band indicates that the water ice was once crystalline. Irradiation of the surface by energetic particles can also cause strong alteration of the surface composition (Strazzulla et al. 1991; Brunetto & Roush 2008). Before entering the giant planet region, Centaurs stored in the Kuiper Belt might have suffered from a significant surface irradiation leading to the formation of a crust, which can

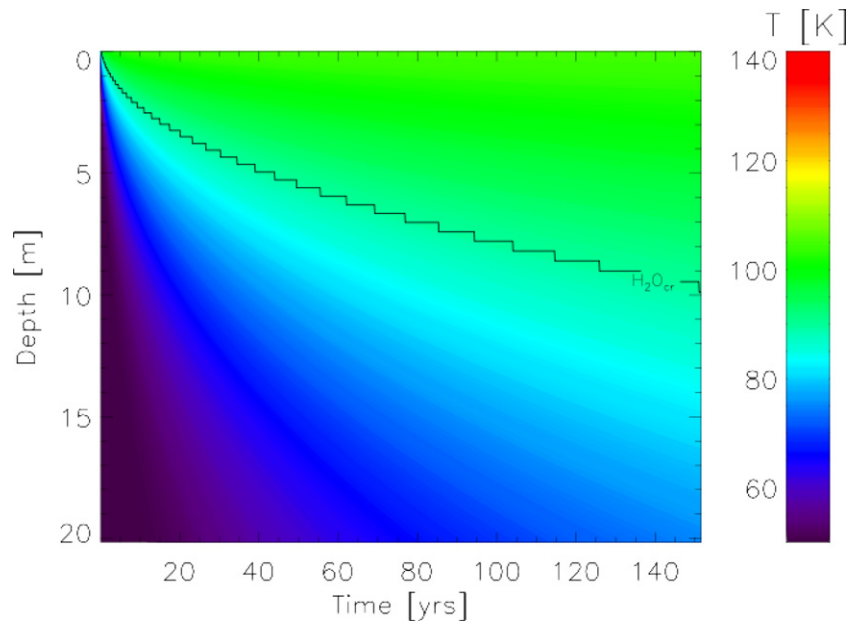


Figure 2. Evolution of the internal temperature distribution below a point at the equator for $a = 8$ AU and $\Theta = 0^\circ$. The black line represents the crystallization front. Time 0 corresponds to the moment when the object is placed on the circular orbit.

(A color version of this figure is available in the online journal.)

easily hide the presence of ices underneath. Therefore, the results from our modeling are not inconsistent with the observations of Centaurs. They provide a motivation for searching for crystalline water ice features at the surface of Centaurs, which could contribute to prove that crystallization is an ongoing process in the giant planet region.

4. CRYSTALLIZATION AS A SOURCE OF COMET-LIKE ACTIVITY

4.1. Internal Propagation of the Crystallization Front

Figures 2–4 show the evolution of the temperature distribution under a specific point of the surface, either pole or on the equator, for $\Theta = 0^\circ$ and $\Theta = 90^\circ$, at 8 AU from the Sun. Time 0 corresponds to the moment when the object is placed on the Centaur orbit, so that we see the propagation of the heat wave from the moment the object reaches a new surface thermal balance in the giant planets region. The heat wave propagates under the surface at a rate that depends on the thermal conductivity. Seasonal effects are observed when $\Theta \neq 0^\circ$, both on the equator (Figure 3) and the pole (Figure 4). Nonetheless, we see that at some depth (comparable to the skin depth), the material is not sensitive anymore to those seasonal effects, meaning that the buried material only feels the mean temperature and no peak variations. Following the heat wave, the crystallization front (black line labeled “H₂O_{cr}” in Figures 2–4) propagates inside the objects. Beyond a distance between 10 and 12 AU, the heat waves are too shallow to significantly induce any crystallization in subsurface layers. The phase transition in those layers is incomplete, and the front remains close to the surface even for large obliquities. Closer to the Sun and for large obliquities, the amorphous/crystalline ice boundary (defined as the boundary between fully amorphous water ice and water ice where crystallization is being triggered) also stops close to the surface (~ 5 –10 m deep). Figure 5 shows the depth of the crystallization front, or in other words the thickness of the crystallized crust for the different (a, Θ) configurations. The phase transition might not be complete above this limit,

especially when the crystallization at the surface is not complete either, e.g., beyond 10–12 AU. This only means that crystalline water ice can be found above this depth.

For $\Theta \neq 0^\circ$, the crystallization front can stop to propagate quite rapidly, within a few orbits. The time depends on the thermal conductivity. This can be explained by the fact that crystallization on the subsurface layers is initiated by the heat wave propagating inward from the surface, which varies due to seasonal effects. If, when the crystalline/amorphous ice boundary is reached, the heat wave carries enough energy to raise the temperature above the crystallization threshold, the phase transition proceeds further inside the object and the boundary moves deeper. Because of seasonal variations of the surface temperature, heat waves are followed by “cool” waves, and later heat waves originating from the surface might be too weak to trigger crystallization at depth. This limit to crystallization is thus greatly favorable to the survival of amorphous water ice inside Centaurs. The amorphous/crystalline phase transition releases trapped molecules which can contribute to an outgassing activity of the object. Specifically, our models suggest that at 6–8 AU the outgassing the crystallization of amorphous ice is limited to a timescale of 10^4 – 10^5 years. Either the crystallization fronts stop propagating (for the reason mentioned above), or they propagate too deep. Indeed, the molecules released by the phase transition have a finite diffusion coefficient $D = 4/3\sqrt{(8k_B T/m\pi)}(\psi^{3/2}r_p)/(1-\psi)^{1/3}$, with k_B the Boltzmann constant, T [K] the temperature and m [kg] the molecule mass, ψ the porosity, and $r_p = 1 \mu\text{m}$ the pore radius (Privalnik 1992). The timescale for seasonal changes being of the order of the year or less, if the crystallization front proceeds deeper than ~ 50 – 100 m, the released molecules are not able to leave the object before a new thermal equilibrium is reached. Beyond 10–12 AU (depending on albedo and thermal conductivity), any cometary activity is very unlikely, as crystallization is barely triggered. When triggered, the phase transition is quenched within a few orbits, in less than 10^3 years. All together, the stopping of the crystallization front propagation and the finite diffusion coefficient of released molecules limit cometary

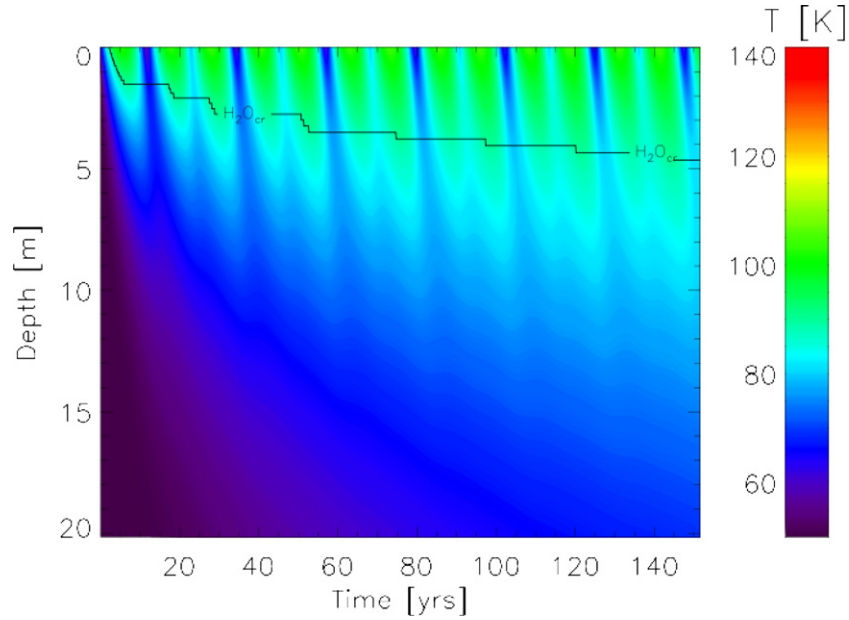


Figure 3. Evolution of the internal temperature distribution below a point at the equator for $a = 8$ AU and $\Theta = 90^\circ$. The black line represents the crystallization front. Time 0 corresponds to the moment when the object is placed on the circular orbit.

(A color version of this figure is available in the online journal.)

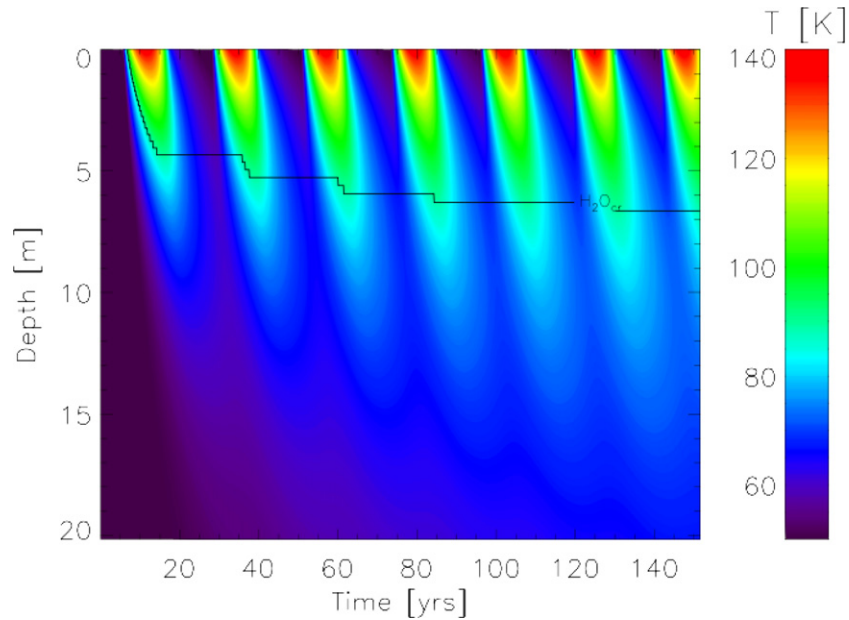


Figure 4. Evolution of the internal temperature distribution below the pole for $a = 8$ AU and $\Theta = 90^\circ$. The black line represents the crystallization front. Time 0 corresponds to the moment when the object is placed on the circular orbit.

(A color version of this figure is available in the online journal.)

activity for 10^5 years at most on any given orbit. The presence of an irradiation crust at the surface of Centaurs (Strazzulla et al. 1991; Hudson et al. 2008), built while they were stored in the Kuiper Belt, could have a damping effect delaying the moment crystallization is triggered inside an object.

Interestingly, in many (a, Θ) configurations (see Figure 5), the amorphous/crystalline ice boundary is close to the surface, so that any additional heat could change the energy balance and trigger sporadic activity. This includes collisions (although the probability for a major impact is close to 0), changes in orbital parameters, internal strains due to close encounters with the giant planets. Also, a progressive erosion can bring the boundary

close enough to the surface for the phase transition to proceed deeper. Eventually, crystallization of amorphous ice can be an efficient source of outgassing for a limited number of (a, Θ) configurations, privileging the small heliocentric distances and small obliquities.

4.2. Observations of Active Centaurs

Among nearly 150 Centaurs detected to date, comet-like activity has been reported for only 16 of them. As shown in Table 3, all active Centaurs except 167P/CINEOS have small perihelion distances, below 9 AU. We also considered for each object the radius $a_c = a(1 - e^2)$ of an equivalent circular

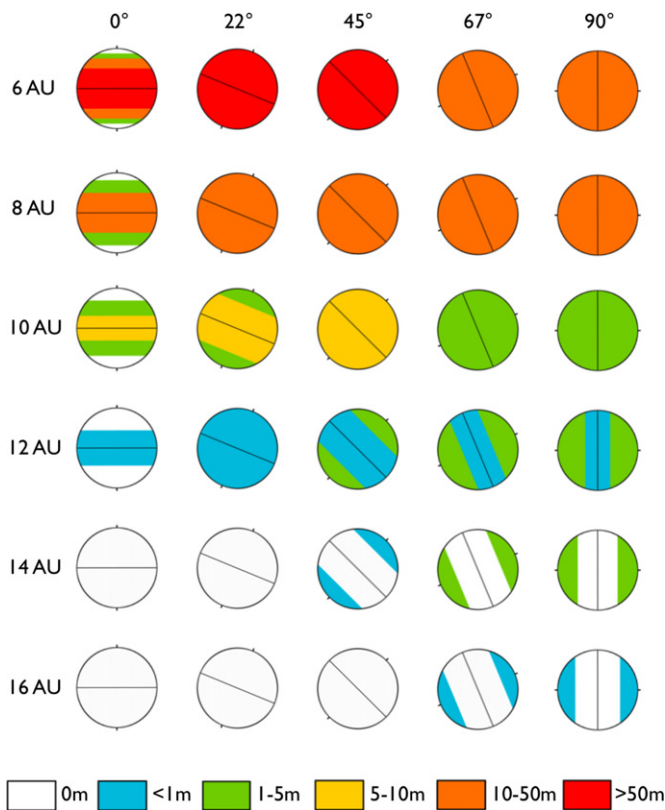


Figure 5. Depths where the crystallization fronts stop for the different (a , Θ) configurations, after 10^5 years. Rows show the different heliocentric distances a , columns display the different obliquities θ . Crystallization may not be complete above these depths, and in many configurations the crystallization front is quenched sooner.

(A color version of this figure is available in the online journal.)

orbit, on which the object would receive the same amount of energy from insolation (Priyalnik & Rosenberg 2009). We show an additional simulation for an elliptic orbit with $a = 11$ AU,

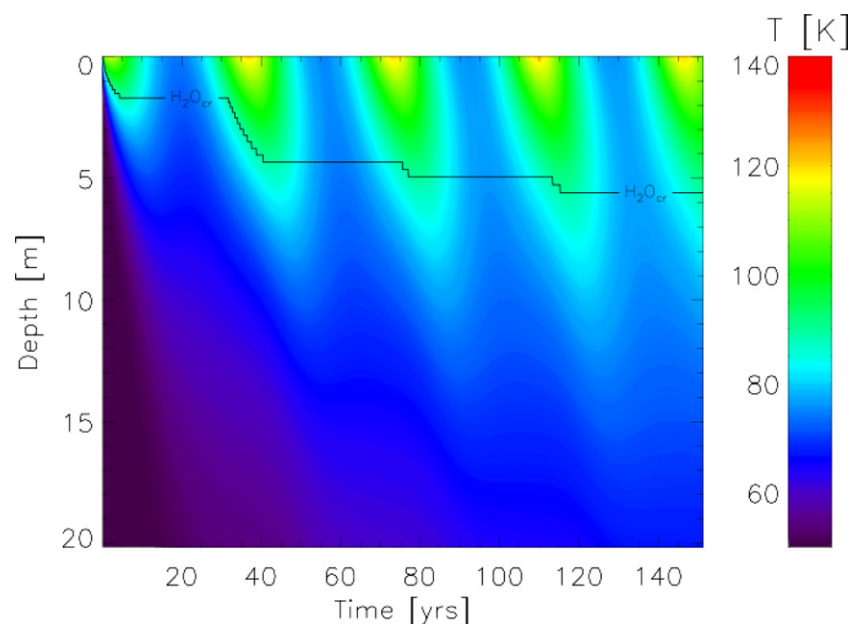


Figure 6. Evolution of the internal temperature distribution below the equator for an elliptic orbit with $a = 11$ AU, $e = 0.45$, $q = 6$ AU, and $a_c = 8$ AU. The black line represents the crystallization front. Time 0 corresponds to the moment when the object is placed on the orbit.

(A color version of this figure is available in the online journal.)

Table 3
Active Centaurs, by Increasing Perihelion Distance

| Designation | a (AU) | e | q (AU) | a_c^a |
|----------------------|-------------|-------|-------------|---------|
| P/2010 C1 (Scotti) | 7.065 | 0.259 | 5.235 | 6.591 |
| C/2001 M10 (NEAT) | 22.656 | 0.801 | 5.302 | 8.119 |
| P/2008 CL94 (Lemmon) | 6.170 | 0.119 | 5.433 | 6.083 |
| P/2004 A1 (LONEOS) | 7.898 | 0.308 | 5.462 | 7.148 |
| 39P/Oterma | 7.251 | 0.245 | 5.471 | 6.815 |
| P/2007 S2 (Lemmon) | 12.548 | 0.557 | 5.558 | 8.655 |
| 29P/S-W 1 | 5.997 | 0.044 | 5.733 | 5.985 |
| (60558) Echeclus | 10.712 | 0.457 | 5.815 | 8.474 |
| P/2010 H5 (Scotti) | 7.144 | 0.156 | 6.026 | 6.970 |
| P/2005 T3 (Read) | 7.511 | 0.174 | 6.200 | 7.283 |
| P/2005 S2 (Skiff) | 7.964 | 0.196 | 6.398 | 7.658 |
| 165P/LINEAR | 18.049 | 0.621 | 6.830 | 11.088 |
| 2003 QD112 | 19.090 | 0.580 | 8.001 | 12.668 |
| (2060) Chiron | 13.670 | 0.379 | 8.486 | 11.706 |
| 166P/NEAT | 13.882 | 0.383 | 8.564 | 11.845 |
| 167P/CINEOS | 16.140 | 0.269 | 11.783 | 14.972 |

Note. ^a $a_c = a(1 - e^2)$ is the radius of a circular orbit receiving the same energy per orbit from isolation.

$e = 0.45$, $q = 6$ AU, and $a_c = 8$ AU ($\Theta = 0^\circ$) as an example of this effect. The results (see Figure 6) suggest that the propagation of the heat wave and crystallization front is similar to that of the 8 AU circular orbit, rather than the 6 AU circular orbit, which is consistent with the idea that the important factor for the evolution is the amount of energy received from insolation per orbit. After a perihelion passage, the heat wave stops propagating, and later heat waves originating from the surface could be too weak to retrigger crystallization. This radius a_c is therefore relevant to allow a direct comparison of observations with our modeling results. The a_c radii of active Centaurs are broadly consistent with the 12 AU limit found by our thermal evolution modeling, meaning that their activity could indeed be caused by the crystallization of amorphous ice.

The most extreme case is 167P/CINEOS, which would barely crystallize in our simulations. Observations of active Centaurs are, however, still limited, as for most objects, the presence of a coma was reported when the object itself was detected. The most striking observation is that active Centaurs share similar orbits with non-active objects. The reason might be related to different compositions owing to different birthplaces in the protoplanetary disk. Different activities could also be due to heterogeneous internal compositions: objects could be active only if/when a pocket or layer of volatiles is reached by the heat wave. This could also be the result of different dynamical histories, as well as different early thermal evolution that can modify the objects initial composition and internal structure.

Our simulations suggest that outgassing due to crystallization of amorphous water ice can only be sustained for a limited amount of time in the giant planet region, leading to the hypothesis that active Centaurs might have “young” orbits. Several examples can support this hypothesis. Centaur P/2010 C1 (Scotti) has had a chaotic dynamical history, leading to a great decrease of its perihelion distance and semimajor axis to the current values (Mazzotta Epifani et al. 2011). The orbital parameters of 39P/Oterma have been modified on the timescale of decades due to close encounters with Jupiter in 1963 (Fernandez et al. 2001). The orbit of Centaur P/2004 A1 (LONEOS) has recently evolved, due to a close passage to Saturn in 1992 (Hahn et al. 2006). In fact, according to Horner et al. (2004), all active Centaurs have short lifetimes on their current orbit. While adjusting to new thermal conditions, the objects could display some cometary activity. The current fraction of active Centaurs $f \sim 10^{-1}$ is of the order of $\tau_{\text{act}}/\tau_{\text{orb}}$, with $\tau_{\text{act}} = 10^5$ yr the outgassing timescale found by our thermal evolution modeling, and τ_{orb} the average timescale an object can spend on a given orbit in the giant planet region. We find that this timescale should be about 10^6 yr to match the current number of active Centaurs, which is consistent with the results from dynamical simulations by Horner et al. (2004).

5. CONCLUSION

Our three-dimensional thermal evolution modeling on initially amorphous Centaurs shows the following.

1. Crystallization can be triggered even at heliocentric distances as large as 16 AU if objects have a high obliquity ($\Theta > 45^\circ$).
2. Amorphous water ice can nonetheless survive at the surface of Centaurs, especially beyond 10 AU.
3. Being accompanied by the release of trapped volatiles, the phase transition from amorphous to crystalline water ice is an efficient source of outgassing, especially for small heliocentric distances and small obliquities. Cometary activity due to crystallization can be expected below 10–12 AU, which is broadly consistent with the observations of active Centaurs, although 167P/CINEOS is an extreme case that barely crystallizes in our simulations.
4. Amorphous water ice can be preserved inside Centaurs, below a ~ 5 –10 m crystallized crust, in many (a , Θ) configurations.
5. Outgassing due to the crystallization of amorphous ice can only be sustained for a limited amount of time, 10^5 years at most, leading to the hypothesis that active Centaurs might have suffered from a recent change in their orbital parameters.

The author thanks A. Delsanti, D. Jewitt, and N. Peixinho, whose comments and suggestions greatly improved the manuscript. This work was supported by a NASA Herschel grant to David Jewitt.

REFERENCES

- Barkume, K. M., Brown, M. E., & Schaller, E. L. 2008, *AJ*, **135**, 55
- Bar-Nun, A., Herman, G., Laufer, D., & Rappaport, M. L. 1985, *Icarus*, **63**, 317
- Bar-Nun, A., & Owen, T. 1998, in *Solar System Ices*, ed. B. Schmitt, C. de Bergh, & M. Festou (Astrophysics and Space Science Library, Vol. 227; Dordrecht: Kluwer)
- Barucci, M. A., Alvarez-Candal, A., Merlin, F., et al. 2011, *Icarus*, **214**, 297
- Barucci, M. A., Boehnhardt, H., Dotto, E., et al. 2002, *A&A*, **392**, 335
- Barucci, M. A., Lazzarin, M., & Tozzi, G. P. 1999, *AJ*, **117**, 1929
- Bauer, J. M., Meech, K. J., Fernandez, Y. R., Farnham, T. L., & Roush, T. L. 2002, *PASP*, **114**, 1309
- Brown, M. E., & Koresko, C. C. 1998, *ApJ*, **505**, L65
- Brown, R. H., Cruikshank, D. P., Pendleton, Y., et al. 1998, *Science*, **280**, 1430
- Brunetto, R., & Roush, T. L. 2008, *A&A*, **481**, 879
- Cruikshank, D. P., Roush, T. L., Bartholomew, M. J., et al. 1998, *Icarus*, **135**, 389
- Davies, J. K., Sykes, M. V., & Cruikshank, D. P. 1993, *Icarus*, **102**, 166
- DeMeo, F. E., Barucci, M. A., Merlin, F., et al. 2010, *A&A*, **521**, 35
- di Sisto, R. P., & Brunini, A. 2007, *Icarus*, **190**, 224
- Doressoundiram, A., Barucci, M. A., Tozzi, G. P., et al. 2005, *Planet. Space Sci.*, **53**, 1501
- Doressoundiram, A., Tozzi, G. P., Barucci, M. A., et al. 2003, *AJ*, **125**, 2721
- Dotto, E., Barucci, M. A., & de Bergh, C. 2003a, *Earth Moon Planets*, **92**, 157
- Dotto, E., Barucci, M. A., Leyrat, C., et al. 2003b, *Icarus*, **164**, 122
- Ellsworth, K., & Schubert, G. 1983, *Icarus*, **54**, 490
- Fernandez, Y. P., Meech, K. J., Pittichova, J., et al. 2001, *IAU Circ.*, **7689**, 3
- Foster, M. J., Green, S. F., McBride, N., & Davies, J. K. 1999, *Icarus*, **141**, 408
- Giauque, W. F., & Stout, J. W. 1936, *J. Am. Chem. Soc.*, **58**, 1144
- Guilbert, A., Alvarez-Candal, A., Merlin, F., et al. 2009a, *Icarus*, **201**, 272
- Guilbert, A., Barucci, M. A., Brunetto, R., et al. 2009b, *A&A*, **501**, 777
- Guilbert-Lepoutre, A., Lasue, J., Federico, C., et al. 2011, *A&A*, **529**, A71
- Hahn, G., Lagerkvist, C.-I., Karlsson, O., Oja, T., & Stoss, R. 2006, *Astron. Nachr.*, **327**, 17
- Horner, J., Evans, N. W., & Bailey, M. E. 2004, *MNRAS*, **354**, 798
- Horner, J., & Lykawka, P. S. 2010, *MNRAS*, **402**, 13
- Hudson, R. L., & Donn, B. 1991, *Icarus*, **94**, 326
- Hudson, R. L., Palumbo, M. E., Strazzulla, G., et al. 2008, in *The Solar System Beyond Neptune*, ed. M. A. Barucci, H. Boehnhardt, D. P. Cruikshank, & A. Morbidelli (Tucson, AZ: Univ. Arizona Press), 507
- Huebner, W. F., Benkhoff, J., & Capria, M. T., et al. (ed.) 2006, *Heat and Gas Diffusion in Comet Nuclei* (Published for The International Space Science Institute; Noordwijk: ESA)
- Jenniskens, P., & Blake, D. F. 1994, *Science*, **265**, 753
- Jewitt, D. 2009, *AJ*, **137**, 4296
- Klinger, J. 1980, *Science*, **209**, 271
- Klinger, J. 1981, *Icarus*, **47**, 320
- Laufer, D., Kochavi, E., & Bar-Nun, A. 1987, *Phys. Rev. B*, **36**, 9219
- Levison, H. F., & Duncan, M. J. 1997, *Icarus*, **127**, 13
- Licandro, J., & Pinilla-Alonso, N. 2005, *ApJ*, **630**, 93
- Luu, J., Jewitt, D., & Cloutis, E. 1994, *Icarus*, **109**, 133
- Luu, J., Jewitt, D., & Trujillo, C. 2000, *ApJ*, **531**, 151
- Mastrapa, R. M. E., & Brown, R. H. 2006, *Icarus*, **183**, 207
- Mazzotta Epifani, E., Perna, D., Licandro, J., et al. 2011, EPSC-DPS Joint Meeting, **2011**, 667
- Meech, K. J., Pittichova, J., Bar-Nun, A., et al. 2009, *Icarus*, **201**, 719
- Merlin, F., Barucci, M. A., Dotto, E., et al. 2005, *A&A*, **444**, 977
- Notesco, G., & Bar-Nun, A. 1996, *Icarus*, **122**, 118
- Notesco, G., Bar-Nun, A., & Owen, T. 2003, *Icarus*, **162**, 183
- Prialnik, D. 1992, *ApJ*, **388**, 196
- Prialnik, D., & Rosenberg, E. D. 2009, *MNRAS*, **399**, 79
- Romon-Martin, J., Delahodde, C., Barucci, M. A., et al. 2003, *A&A*, **400**, 369
- Schmitt, B., Espinasse, S., Grim, R. J. A., Greenberg, J. M., & Klinger, J. 1989, *Phys. Mech. Cometary Mater.*, **302**, 65
- Stansberry, J., Grundy, W., Brown, M., et al. 2008, in *The Solar System Beyond Neptune*, ed. M. A. Barucci, H. Boehnhardt, D. Cruikshank, & A. Morbidelli (Tucson, AZ: Univ. Arizona Press), 592 pp. 161
- Strazzulla, G., Baratta, G. A., Johnson, R. E., et al. 1991, *Icarus*, **91**, 101
- Tiscareno, M. S., & Malhotra, R. 2003, *AJ*, **126**, 3122
- Volk, K., & Malhotra, R. 2008, *ApJ*, **687**, 714